This article has been accepted for inclusion in a future issue of this journal. Content is final as presented, with the exception of pagination.

Generation and Quality Assessment of Stereo-Extracted DSM from GeoEye-1 and WorldView-2 Imagery

Manuel Ángel Aguilar, María del Mar Saldaña, and Fernando José Aguilar

***Abstract*—Digital surface models (DSMs) extracted from 15 different stereo pairs attained by the combination of GeoEye-1 (GE1) and WorldView-2 (WV2) panchromatic very high resolution (VHR) satellite images are tested. Two of them are pure same-date along-track stereo pairs, one from each VHR satellite, whereas the rest are mixed multidate across-track ones. A quality assessment on the DSMs extracted from the aforementioned stereo pairs, involving both accuracy and completeness, is carried out. Several factors are tested such as sensor model used in the bundle adjustment, number of ground control points (GCPs), radiometric characteristics, satellite imaging geometry, time between acquisition dates, and target land cover. A highly accurate light detection and ranging elevation data is used as ground truth. Overall, 3-D rational functions refined by a zero-order polynomial adjustment by using 7 or 12 GCPs performed slightly better regarding both DSM vertical accuracy and completeness. In relation to the pure stereo pairs, the DSM extracted from the GE1 stereo pair attained better vertical accuracy over the whole study area (90th percentile linear error, LE90, of 2.04 m) but lower completeness (74.50%) than the WV2 one (2.56 m and 83.35%, respectively). The undergoing hypothesis is that the blurrier images from WV2 could have influenced in the improvement of the matching success rate while reducing the vertical accuracy of extracted points. When all the 15 stereo pairs are considered, the vertical accuracy mainly depends on the convergence angle. In addition, the temporal difference between acquisition dates turned out to be the most influential factor regarding completeness values.**

***Index Terms*—Accuracy, digital elevation models (DEM), earth observing system, error analysis, satellites, terrain mapping.**

I. Introduction

An ENTIRELY new age in remote sensing began with the launch of IKONOS in September 1999. It is the first of a new breed of commercial very high resolution (VHR) optical satellites capable of capturing panchromatic (PAN) images of the Earth surface with a ground sample distance (GSD) of 1 m, and even less. Optical VHR satellites have proven their ability to provide accurate cartographic products such as orthoimages [1]–[4] and digital surface models (DSMs) [5]–[9].

Manuscript received July 27, 2012; revised February 4, 2013; accepted February 19, 2013. This work was supported by the Spanish Ministry for Science and Innovation (Spanish Government), the European Union (FEDER founds) under Grant Reference CTM2010-16573, and the Andalusia Regional Government, Spain, through the Excellence Research Project RNM-3575.

The authors are with the Department of Engineering, Almeria University, Almeria 04120, Spain (e-mail: maguilar@ual.es; msd452@ual.es; faguilar@ual.es).

Color versions of one or more of the figures in this paper are available online at http://ieeexplore.ieee.org.

Digital Object Identifier 10.1109/TGRS.2013.2249521

On the one hand, the adaptable stereo imaging capability of the newest civilian VHR satellites allows generating strong stereo geometry with base-to-height ratio (B/H) >0.5. Satellite imaging geometry, in particular B/H ratio or convergence angle, plays a significant role in the improvement of DSM vertical accuracy [10], [11], although smaller B/H ratios may be preferred in city areas to increase similarity between the two stereo images and thus improving the matching stage [7]. In addition, their agile pointing ability enables the generation of same-date in-track stereo images, reducing radiometric image variations and so improving the success rate in any matching process [5], [12]. In this way, VHR stereo data can be quickly acquired from almost any location on Earth, with a short revisit time and at a reasonable cost. The extraction of 3-D information from VHR satellite sensor imagery is the subject of a large photogrammetric investigation for the last decade, mainly conducted in three ways.

1) Testing different physical and empirical sensor models at the triangulation phase [9], [13]–[22].
2) Comparing DSM accuracies from different pure VHR satellite stereo pairs. It means stereo imagery products in which both images are collected by the same sensor at the same date, along-track path, and presenting optimal angles for stereo viewing [5], [9], [15]. It would also comprise mixed stereo pairs that combine single across-track images from both the same or different sensors [10], [11].
3) Comparing different automatic DSM generation modules [6], [7], [9], [17] or different matching algorithms for DSM generation [22]–[24].

GeoEye-1 (GE1) (GeoEye, Inc.), launched in 2008, is currently the commercial VHR satellite with the highest geometric resolution, both in PAN and multispectral (MS) products (nominal GSD at nadir of 0.41 and 1.65 m, respectively). WorldView-2 (WV2) (DigitalGlobe, Inc.), launched in October 2009, and with 0.46 and 1.84 m nominal resolution at nadir in PAN and MS, respectively, was the first commercial VHR satellite to offer 8-MS bands. All the image products from GE1 and WV2 have to be down-sampled to 0.5 and 2 m in PAN and MS, respectively, for commercial sales, as a requirement levied by the U.S. Government. Nowadays GE1 and WV2 are the two commercial VHR satellites more innovative and unexplored. In this way, the first vertical accuracy results attained from GE1 and WV2 PAN stereo pairs, although quite variable, are superior enough to those obtained from older satellites such as IKONOS, QuickBird or WorldView-1 (WV1). For example, Mitchell and MacNabb [25] reported vertical accuracies of 0.25 m (measured as standard deviation) working with a GE1 stereo pair. A similar vertical accuracy is reported by Fraser and Ravanbakhsh [16], but now expressed as root mean squared error ($RMSE_z$). Much higher $RMSE_z$ values of ~0.44 and 0.7 m are attained by Wang and Zhao [26] as well as Meguro and Fraser [27], respectively. On the other hand, and using WV2 stereo pairs, a standard deviation value of 0.31 m is brought out by Mitchell and MacNabb [25], whereas a value of 1.20 m ($RMSE_z$) is attained by Hobi and Ginzler [28] working on herb and grass land cover. Usually, the specification of accuracy measures is based on the assumption that the errors follow a Gaussian distribution and that no outliers exist. However, this is frequently not the case, due to the presence of objects above the terrain, such as vegetation, buildings, and unwanted objects (cars, people, animals, and so on). Therefore, there is an increasing trend to propose robust and nonparametric statistical methods to estimate the accuracy of DSMs under non-open terrain, where error distribution is usually far away from the normal distribution [29]. In robust statistical methods such as sample quantiles of the absolute errors should be used as accuracy measures [30]. Nevertheless, apart from sample data accuracy, density, and distribution of the source data, DSM accuracy also depends on the roughness of the terrain surface [31], [32] and the target land cover [15], [28], [33].

The procedure for assessing digital elevation model (DEM) or DSM quality involves examination of the vertical accuracy and completeness [34], [35]. DSM vertical accuracy could be attained by computing height differences between independently surveyed check points and planimetrically corresponding DSM points. Independent check points (ICPs) should be at least three times more accurate than the expected accuracy to be verified and the minimum required sample size to assure a reliable accuracy assessment is not easy to specify [36]. In addition, they have to cover the whole working area. Considering all those aforementioned shortcomings, many researchers proposed the use of a highly accurate light detection and ranging (LiDAR)-derived DSM as ground truth to check the accuracy of DSM generated from VHR satellite images [5], [9], [15], [25]. Bearing in mind that the automatic DSM cannot be determined in all areas because of matching errors provoked by insufficient texture, occlusions or radiometric artifacts, DSM accuracy should be complemented by DSM completeness, which can be defined as the percentage of correctly matched points over the working area or, in other words, the amount of missing area in relation to the whole working area [35].

The objectives of this paper are to evaluate and compare the DSMs extracted from pure along-track GE1 and WV2 PAN VHR satellite stereo pairs, exactly in the same working area and conditions, by using a highly accurate LiDAR-derived DSM as ground truth. DSMs are also derived from different stereo combinations (mixed stereo pairs) of GE1 and WV2 single images. Thus, the goal of this paper is to evaluate the effect on DSM vertical accuracy and completeness of several factors such as: 1) sensor model; 2) number of ground control points (GCPs); 3) radiometric characteristics of each single VHR satellite image; 4) time between acquisition dates; 5) target land cover; and 6) imaging geometry.

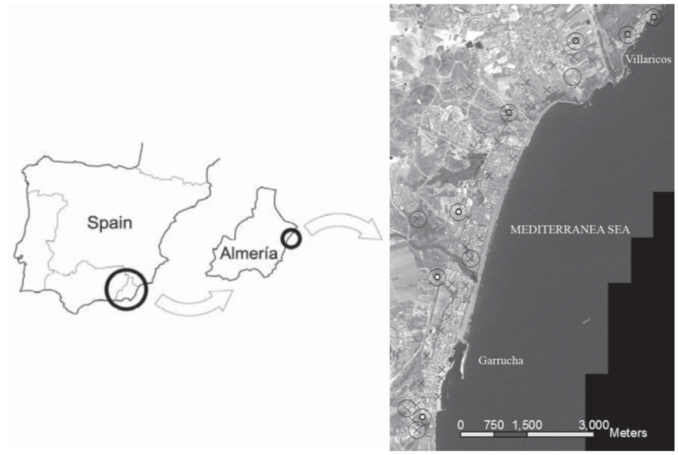

Fig. 1. Location of the study site on the Almería coast, Spain, and distribution of 45 GCPs (crosses), 12 GCPs (big circles) and 7 GCPs (little circles) overlaid on a GE1 PAN orthoimage.

II. Study Site and Datasets

A. Study Site

The study area is centered on WGS84 geographic coordinates of 37.2109° North and 1.8027° West (Fig. 1). The study area, located between the harbors of Garrucha and Villaricos (Southern Spain), presents heights above mean sea level ranging from 0 to 55 m and a mean value close to 7 m.

B. GE1 VHR Satellite Data

GE1 Geo is the GeoEye's commercial imagery format that presents least level of processing, both radiometric and geometric corrections. Geo images are shipped with the sensor camera model in rational polynomial coefficients (RPC) format and a metadata file where the most relevant physical parameters of the image are summarized [37].

For this experiment, three PAN GE1 Geo images are acquired with a final 0.5-m GSD (Table I). These images are ordered with a dynamic range of 11-bit and without the application of the dynamic range adjustment (DRA) preprocessing (i.e., maintaining absolute radiometric accuracy and full dynamic range for scientific applications). The three images from GE1 used 16 time delay and integration (TDI) stages. The first one was taken on September 29, 2010, approximately covering 49 km^2. On August 27, 2011, a GE1 GeoStereo product (pure stereo pair) was taken, containing two images that counted on the appropriate stereo geometry to support a wide range of stereo imagery applications such as DSMs creation. In a single image, GeoStereo product is identical to Geo product.

C. WV2 VHR Satellite Data

Ortho Ready Standard Level-2A (ORS2A) imagery [38] is addressed as the best DigitalGlobe's format to produce

TABLE I
CHARACTERISTICS OF PAN IMAGES FROM GE1 (GEO AND GEOSTEREO PRODUCTS) AND WV2 (ORS2A) ACQUIRED AT THE STUDY SITE

Image ID	GE11	GE12	GE13	WV21	WV22	WV23
Product	GE1 Geo	GE1 GeoStereo	GE1 GeoStereo	WV2 ORS2A	WV2 ORS2A	WV2 ORS2A
Acquisition date	29/9/2010	27/8/2011	27/8/2011	19/7/2011	18/8/2011	18/8/2011
Acquisition time (GTM)	11:01	10:55	10:56	11:23	11:22	11:23
Cloud cover	0%	0%	0%	0%	0%	0%
Scan direction	Reverse	Reverse	Reverse	Forward	Forward	Reverse
Sun azimuth	159.3°	144.1°	144.4°	142.5°	152.3°	152.8°
Sun elevation	48.4°	58.3°	58.4°	70.5°	63.7°	63.8°
Collection elevation	69.4°	81.5°	66.9°	85.0°	67.6°	80.0°
Collection azimuth	221.9°	40.4°	183.6°	279.9°	4.7°	216.1°
Collected col GSD	0.460 m	0.416 m	0.480 m	0.467 m	0.499 m	0.473 m
Collected row GSD	0.449 m	0.417 m	0.440 m	0.465 m	0.538 m	0.480 m
Product pixel size	0.5 m	0.5 m	0.5 m	0.5 m	0.5 m	0.5 m

highly accurate orthorectified products and DSMs from both WV1 [39] and WV2 [40]. WV2 ORS2A images present both radiometric and geometric corrections in a similar level to the GeoEye's Geo format. ORS2A images are georeferenced to a cartographic projection using a surface with constant height and, as in GeoEye's Geo level, they include the corresponding RPC sensor camera model and metadata file.

Three 0.5-GSD PAN WV2 ORS2A images are acquired over the working area (Table I). The delivered products, without any enhancement (no DRA) and employing 32 TDI stages, presented a real dynamic range of 11-bit. The first single ORS2A image was taken on July 19, 2011, whereas a pure WV2 stereo pair, containing two ORS2A images, was acquired on August 18, 2011.

D. Ground Points Collection and LiDAR Data

The ground point coordinates are obtained by differential global positioning system (DGPS) by means of a total GPS Topcon HiPer PRO station working in real time kinematic mode and using the satellite's carrier. The DGPS works are supported by 11 survey points from both the Spanish National Geodetic Network and the Network of Environmental Information of Andalusia (Spain). After adjusting the survey network, the RMSE values finally obtained at these known points turned out to be of 0.056, 0.033, and 0.076 m in x, y, and z-axes, respectively. Thus, the coordinates of 120 ground points, located at well-defined features and homogeneously distributed over the entire study area (Fig. 1), are surveyed and referenced to ETRS89 (UTM projection). The geoid based on the global Earth Gravitational Model of 1996 (EGM96) is used for attaining the final orthometric heights. The goal is to obtain a reliable measurement of GCPs and ICPs providing position accuracy at better than 10 cm. From these ground points, 51 are selected as GCPs and the remaining 69 are used as ICPs.

A high accuracy and resolution LiDAR-derived DSM with an irregular-spacing grid and orthometric heights (EGM96) is also used in this paper as ground truth. It was taken on August 30, 2011, as a combined photogrammetric and LiDAR survey at a flying height above ground of ~350 m. A helicopter mounted laser scanner system developed by AeroLaser System S.L. based on a Riegl LMS Q240i and with 30° field of view is used, attaining an average point density >2 points/m^2.

The estimated vertical accuracy of the LiDAR-derived DSM is computed on 37 DGPS ground points located in open areas, resulting in a value of 0.085 m (measured as RMSE). The LiDAR vertical accuracy is finally very close to the one attained at the DGPS points.

TABLE II
IMAGING GEOMETRY, SUN POSITION DISCREPANCIES AND DIFFERENCE BETWEEN ACQUISITION DATES OF EACH CONSIDERED STEREO PAIR FROM THE SIX ORIGINAL PAN SINGLE IMAGES DESCRIBED IN TABLE I

ID	Image Combination	Convergence Angle (Degrees)	Sun Convergence Angle (Degrees)	Base / Height Ratio	Difference in Acquisition Date (Days)
1	GE12-GE13	30.39	0.19	0.55	0
2	WV22-WV23	31.35	0.24	0.57	0
3	GE13-WV23	15.62	6.74	0.26	9
4	GE13-WV22	45.55	6.53	0.84	9
5	GE12-WV23	18.52	6.91	0.33	9
6	GE12-WV22	16.21	6.69	0.33	9
7	WV21-WV22	22.48	7.77	0.41	29
8	WV21-WV23	8.98	7.78	0.16	29
9	GE13-WV21	24.19	12.13	0.42	38
10	GE12-WV21	11.87	12.22	0.20	38
11	WV21-GE11	18.41	23.50	0.28	295
12	WV23-GE11	10.69	15.80	0.17	324
13	WV22-GE11	40.64	15.77	0.70	324
14	GE13-GE11	14.25	13.32	0.27	333
15	GE12-GE11	29.12	13.37	0.53	333

III. METHODOLOGY

A. Considered Stereo Pairs

Combining the six original PAN single images shown in Table I, 15 different stereo pairs could be made up (Table II). For each stereo pair, Table II shows the main factors that could affect the accuracy and/or completeness results such as stereo imaging geometry (measured as convergence angle or B/H ratio), difference between acquisition dates of the images making up the stereo pair and, finally changes in the light source position. Obviously, and in across-track stereo pairs, the greater the time difference between the images, the higher the probability of spectral and spatial differences between those images. Changes in cloud cover, vegetation, glints on water bodies, and so on, they will all contribute to correlation problems. The same could be said about sun position.

With regard to stereo imaging geometry, the convergence angle can be defined as the angle between two rays that intersect at a common ground point, one from the fore image and one from the aft image, measured along the convergence or epipolar plane. In addition, the B/H ratio is defined by the separation of the pair divided by the height of the sensor. Theoretically, an angle between 30° and 60° would be ideal whereas a B/H ratio between 0.5 and 1.0 is usually the most appropriate for DEM creation.

In this sense, the convergence angle, δ, between every two images [10] that have nominal elevation angle and nominal collection azimuth values of (α_1, θ_1) and (α_2, θ_2) can be calculated as follows:

$$\cos\delta = \sin\alpha_1 \cdot \sin\alpha_2 + \cos\alpha_1 \cdot \cos\alpha_2 \cdot \cos(\theta_1 - \theta_2). \quad (1)$$

As a measure of the difference between the light source positions for every stereo pair, the sun convergence angle is calculated by applying (1), although in this case using sun azimuth and sun elevation values, respectively. The pure along-track stereo pairs from GE1 and WV2 (ID 1 and 2, respectively, in Table II) presented a very similar configuration with convergence angles close to 30° and without any practical difference in relation to illumination conditions.

B. DSM Extraction from VHR Satellite Imagery

The first step for extracting an accurate DSM from VHR satellite stereo pairs is carried out by means of the bundle adjustment based on 3-D GCPs. In the last decades, several mathematical models for VHR satellite sensor orientation and 3-D geopositioning are tested. These models can be categorized into two main groups: 1) 3-D rigorous or physical mathematical models and 2) empirical models. OrthoEngine^{SE} from Geomatica v. 2012, developed by PCI Geomatics (PCI Geomatics, Richmond Hill, Ontario, Canada), is the photogrammetric software package used in this experiment for testing the following types of sensor models.

1) A 3-D physical model developed by Toutin [14] at the Canada Center for Remote Sensing (CCRS). A solution for CCRS model can be obtained through a limited number of GCPs (∼six to eight).
2) An empirical model based on a third-order 3-D rational functions with vendor's RPCs data and refined by a zero-order polynomial adjustment (RPC0), following the block adjustment method published by Grodecki and Dial [41] for image space. RPC0 requires only one GCP in principle; anyway, to have a better reliability, more than one GCP are applied here.

RPC0 sensor model is pointed out as the sensor model offering the best orientation accuracy when working on PAN WV2 imagery [22]. In the last work, several software packages (Geomatica, ERDAS Imagine, and SISAR software) are tested using both rigorous and empirical models, proving that orientation accuracy is practically software independent. That is the main reason for using only a unique, widely known, off-the-shelf software in this experiment. RPC0 also yielded better results than CCRS for single PAN images of GE1 and WV2 [40]. However that could change when dealing with stereo pairs. In RPC0, OrthoEngine computes each image individually by using the marked GCPs but, actually, there is no 3-D relative orientation or stereo-bundle adjustment to compensate image space residuals for both images at the same time. In other words, the coefficients computed for each image making up a stereo pair project are the same that those ones coming from computing separately each single image. That is obviously true when both projects are supported by the same GCPs. On the contrary, a real stereo-bundle adjustment (3-D intersection) between both stereo images is undertaken when CCRS model is applied [42].

Regarding GCPs, although a number around four is recommended for RPC0 [16], [22], statistically significant improvements working with WV2 single PAN images are found by using seven GCPs [40]. Thus, three different sets of 7, 12, and 45 well-distributed GCPs are tested (Fig. 1). The accuracy of the sensor orientation phase is always controlled at the same remaining 69 ICPs. In this way, and for RPC0, RMSE along x and y-axes after sensor orientation phase is computed for each combination of sensor model and number of CGPs tested, whereas a complete accuracy report including vertical RMSE (i.e., a real stereo-bundle adjustment) is attained from CCRS model. In 7 and 12 GCPs, the ground points are all located on open terrain. In 45 GCPs, some of them are located on roofs, buildings or other elevated structures. When ground points are located on elevated structures, a little error in the introduction of photo coordinates could provoke a significant error in heights. It is important to keep in mind that, for each image tested, the ground points (GCPs and ICPs) are only marked once. Therefore the pointing error in image space would be the same for all projects. In this way, the bundle adjustment for every stereo pair shown in Table II is carried out by using four different strategies: 1) applying RPC0 sensor model and the set of seven GCPs; 2) RPC0 with 12 GCPs; 3) CCRS with 12 GCPs; and 4) CCRS with 45 GCPs.

After carrying out the bundle adjustment phase, OrthoEngine is used for DSM extraction. In this sense, an automated area-based matching procedure is performed on quasi-epipolar images. This procedure is based on a hierarchical (seven steps) subpixel mean normalized cross correlation matching method that generates correlation coefficients between zero and one for each matched pixel, where zero is a total mismatch and one is a perfect match. When the correlation coefficient of a matched point is < 0.5, this point is rejected and its height is not computed, so meaning a gap and reducing the DSM completeness. Finally, a second-order surface is then fitted around the maximum correlation coefficients to find the match position to subpixel accuracy [39]. Only sampling interval and level of detail are the parameters that can be adjusted by the user in OrthoEngine DSM extraction module. For every

Fig. 2. Different areas for assessing the quality of DSMs overlaid on a GE1 orthoimage. Urban areas in white, unchanged areas in solid black and the whole working area in black dashed line.

DSM, the epipolar images are generated at a sampling distance of 0.5 m (down sample factor of one). In this way, a high detail DSM with 32 bits and a pixel sampling factor of two are selected into OrthoEngine, thereby generating 1-m grid-spacing DSMs. Due to DSMs extracted by OrthoEngine are referenced to WGS84 ellipsoid, the EGM96 geoid had to be used for attaining the final orthometric heights. No further editing is applied on the DSMs.

C. Assessing the Quality of DSMs

The quality of the extracted DSMs is assessed in two ways: 1) vertical accuracy and 2) completeness. Considering that the vertical accuracy and completeness of a DSM largely depend on the target land cover, three different areas are considered for assessing the quality of the DSMs extracted from VHR satellite imagery: 1) the whole working area; 2) unchanged areas; and 3) urban areas (Fig. 2). In any event, the previously described LiDAR-derived DSM is used as ground truth to carry out the accuracy assessment of the DSMs extracted from every stereo pair. The whole working area covered 7.71 km^2 where more than 18 millions of 3-D points are available from LiDAR data. Seven control areas representing urban areas covered $\sim$1.22 km^2, meaning almost three millions of LiDAR points. Finally, 34 flat and unchanged areas over time such as football pitch, basketball or tennis courts and similar, spanning $\sim$0.03 km^2 and presenting $\sim$78 508 LiDAR points. Any editing process is applied on DSMs from VHR satellite imagery and, in addition, the matching gaps are not filled.

In vertical accuracy assessment undertaken over the whole working area, the LiDAR-derived DSM is interpolated to 1-m grid spacing by using linear triangulation. Once gridded, it is employed as ground truth for the vertical accuracy assessment of the raw DSMs computed from VHR satellite images. The applied sensor model is RPC0 supported by 12 GCPs. After removing blunder errors from the residuals populations (z-residuals) by applying the widely known three-sigma rule [43], measures such as mean, standard deviation, 90th (LE90), and 95th (LE95) percentile linear error are computed for the final vertical accuracy assessment.

To know the vertical accuracy of the extracted DSMs in urban areas, a test over 93 000 m^2 of a representative urban area situated in the village of Villaricos (located at the north of the working area) is undertaken following the same procedure already described for the entire area.

Regarding unchanged areas, the interpolation from the LiDAR point cloud (irregularly spaced points) is carried out by using the Delaunay triangulation process included in RapidForm (INUS Technology Inc., Seoul, Korea). In this way, the original point cloud is not changed and so the interpolation errors are minimized. RapidForm is used to compare the LiDAR ground truth and the different DSMs from VHR satellite imagery. From this comparison, the statistics corresponding to the signed z-differences between ground truth and the different DSMs are computed. RapidForm only reports values of mean and standard deviation when it computes the distance deviation between two DSMs. So, the computed values of z-differences are not available for further analysis (e.g., LE90 or LE95). Again the three-sigma rule [43] is used to leave out outliers from the final statistical evaluation. For all accuracy tests, height differences are computed by comparing the reference LiDAR DSM over the analyzed DSM (the value is positive when the VHR satellite-derived DSM is above the LiDAR DSM).

In addition to accuracy assessment, completeness of DSMs is also computed for the different studied areas. DSM points could not be determined in all areas mainly because of matching process failure (when correlation coefficients are < 0.5 in OrthoEngine). Thus, the ratio between the number of correctly matched points and the maximum possible number of points (given in percent) offers a quantitative measure of DSM completeness.

IV. Results

A. DSM Accuracy

The vertical accuracy assessment of the DSMs extracted from VHR satellite stereo pairs is carried out both at 69 ICPs after the stereo-bundle adjustment and also by using a LiDAR-derived DSM as ground truth over the 34 flat and unchanged areas previously described. Table III shows the RMSE at ICPs for the projects using same-time along-track (i.e., pure)

TABLE III
RESULTS OF STEREO-BUNDLE ADJUSTMENT FOR THE SAME-TIME ALONG-TRACK STEREO PAIRS FROM GE1 AND WV2 (ID 1 AND 2), AND STATISTICAL RESULTS (MEAN AND STANDARD DEVIATION) FROM THE COMPARISON OF BOTH DSMS WITH LIDAR ELEVATION DATA OVER UNCHANGED AREAS

Stereo Pair	Sensor Model	No. GCPs	RMSE on 69 ICPs (m) Bundle Adjustment Stage				LiDAR – VHRS DSM (m)	
			X	Y	XY	Z	Mean	σ
ID 1 GE1	RPC0	7	0.29	0.27	0.39	–	0.12	0.40
	RPC0	12	0.27	0.26	0.38	–	0.14	0.39
	CCRS	12	0.28	0.25	0.37	0.57	– 0.02	0.41
	CCRS	45	0.24	0.22	0.33	0.59	0.20	0.43
ID 2 WV2	RPC0	7	0.36	0.37	0.52	–	–0.03	0.53
	RPC0	12	0.34	0.35	0.49	–	–0.09	0.53
	CCRS	12	0.28	0.4	0.49	1.01	–0.24	0.68
	CCRS	45	0.27	0.35	0.44	0.77	0.03	0.64

stereo pairs from both GE1 (ID 1) and WV2 (ID 2). Regarding the effect of sensor models and GCPs on after bundle adjustment planimetric accuracy, the differences are negligible. In addition, when working on the same set of 12 GCPs, the estimated accuracy for RPC0 and CCRS sensor models is practically the same. In single images, RPC0 supported by seven GCPs is clearly better (planimetric accuracies of ∼0.37 and 0.44 m for GE1 and WV2, respectively) than CCRS with 12 GCPs (planimetric accuracies of 0.50 m in GE1 and 0.63 m for WV2) [40], [44]. However, these accuracy differences are greatly reduced by using stereo-bundle adjustment in CCRS sensor model (Table III). Notice that, vertical accuracy at ICPs is not available through the bundle adjustment OrthoEngine report for RPC0 sensor model. Therefore, it is impossible to evaluate the vertical accuracy at sensor orientation stage in RPC0 sensor model (Table III).

Once sensor orientation is computed for the different combinations of sensor models and number of GCPs, every stereo matching-derived DSM is compared with the LiDAR-derived DSM previously described (ground truth) to estimate its vertical accuracy over the unchanged areas. In this way, the differences due to sensor models and number of GCPs regarding vertical accuracy (measured as standard deviation) are practically negligible for GE1. However slightly worse accuracies are achieved for CCRS in the case of WV2. In regard to the studied sensors, more accurate DSMs are attained from the pure stereo pair of GE1 than for the WV2 (average improvement of vertical accuracy close to 0.19 m). DSM vertical accuracies (σ) from GE1 pure stereo pair are slightly better than the mean collected GSD for the original images (0.44 m). In WV2, the mean collected GSD value (0.50 m) is always lesser than the attained accuracy, especially when CCRS model is used. Vertical systematic errors of around ±0.20 m are occasionally found for both sensor models and the pure stereo pairs tested (Table III).

The accuracy assessment tests carried out hitherto are presenting the potentially best planimetric and vertical accuracies from VHR satellite imagery DSMs as they are restricted to flat and unchanged areas. However, it is also important to know the vertical accuracy of the extracted DSMs in both urban areas and the entire working area. In this sense, RPC0 sensor model supported by 12 GCPs is applied in the representative urban test area located at Villaricos. Once removed the outliers, 86 807 (2.11% of outliers removed) and 91 601 (2.09% of outliers) z-residuals for GE1 and WV2 DSMs, respectively, are calculated. From Table IV, the statistical results for the DSM extracted from the pure stereo pairs of GE1 and WV2 turned out to be very similar. Moreover, a visual analysis over a limited area of this test can be shown in Fig. 3, indicating that raw DSMs extracted from VHR satellite images should be strongly edited in urban areas, especially the building edges where the smoothing effect of the DSMs usually generates the highest errors [Fig. 3(f)]. This smoothing effect, already reported by [24], resulted in a significant increase of the systematic error. Moreover, Alobeid *et al.* [24] concluded that the matching method for generating DSMs is crucial in urban environments. They found that the area-based least squares matching is not able to generate clear building outlines and it strongly depends on occlusions. On the other hand, semiglobal matching [45] and dynamic programming matching method [46] achieve the best results working in urban areas.

TABLE IV
STATISTICAL RESULTS FROM THE COMPARISON OF BOTH PURE DSMS (ID 1 AND 2) GENERATED BY USING RPC0 AND 12 GCPS WITH LIDAR ELEVATION DATA OVER DIFFERENT STUDY AREAS

Stereo Pair	Study Area	LiDAR – VHRS DSM (m)			
		Mean	σ	LE90	LE95
ID 1 GE1	Urban area	0.87	2.67	5.05	6.86
	Whole area	0.22	1.32	2.04	3.16
ID 2 WV2	Urban area	1.03	2.74	5.26	7.10
	Whole area	0.12	1.75	2.56	4.06

An accuracy assessment over the whole working area for the pure stereo pairs from both GE1 and WV2 is also carried out by taking the LiDAR-derived DSM as reference. RPC0 supported by 12 GCPs is the sensor model employed. Again, the outliers are removed (2.20 and 1.51% of outliers removed for GE1 and WV2, respectively) before z-residuals are computed (Table IV). For all types of the tested target land covers, the DSM extracted from the pure stereo pair of GE1 yielded better accuracies than the WV2 one.

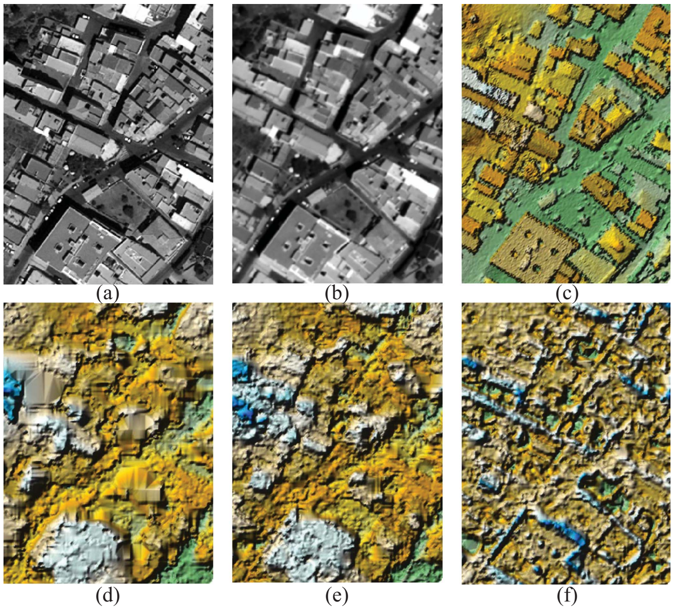

Fig. 3. Visual analysis over a limited urban area (112 × 150 m). (a) GE12 original PAN image. (b) WV23 original PAN image. (c) LiDAR-derived DSM. (d) DSM from GE12-GE13 (ID 1) stereo pair. (e) DSM from WV22-WV23 (ID 2) stereo pair. (f) vertical residuals from the comparison between LiDAR-derived DSM with WV2's DSM.

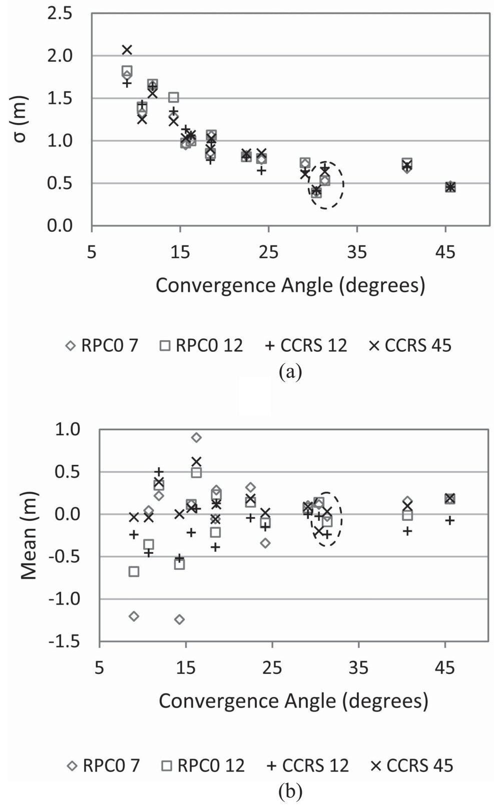

Fig. 4. Relationship between signed z-difference statistics after removing outliers and convergence angle for each stereo pair. (a) Standard deviations. (b) Mean values. All the presented statistics have been computed over unchanged areas. z-differences refer to the height difference between each computed DSM from satellite stereo pair and the LiDAR elevation data. Pure stereo pairs are highlighted by means of a dashed circle.

Fig. 4 is made up to help analyzing the vertical accuracy over unchanged areas of DSMs from every stereo pair considered in this paper (henceforth including pure and mixed ones). In this way, and regarding vertical uncertainty [Fig. 4(a)], it tended to decrease (i.e., more accurate DSM) when increasing the convergence angle (i.e., the stereo pair imaging geometry) as reported in other researches [10], [11]. It should be noted that the vertical accuracy for pure stereo pairs presenting convergence angles of 30.39° (GE1) and 31.35° (WV2), highlighted by means of a dashed circle in Fig. 4(a), turned out to be slightly better than for mixed ones. This is most likely because both pure stereo pairs are taken under ideal conditions, i.e., without any difference between acquisition dates and with almost the same sun position. The main problem when working on mixed stereo pairs is because of radiometric differences between images, which of course are also dependent on differences in acquisition dates. In this sense, a filter to enhance the edges and then to reduce the radiometric errors on the original images that are forming a Cartosat-1 stereo pair is successfully tested by Crespi *et al.* [47] before extracting the DSM. In our case, and without applying any filter, vertical accuracies are ranging from 0.60 to 0.90 m in the mixed stereo pairs with convergence angles between 22° and 30° (i.e., presenting stereo imaging geometry similar to the pure stereo pairs). Turning now to DSMs bias [Fig. 4(b)], convergence angles $< 18°$ or B/H ratios < 0.28 resulted in the highest vertical systematic errors and, in addition, produced more variable values. This is particularly important when the sensor orientation is resolved by using RPC0 with only seven GCPs. Because of that, these extremely weak stereo pair configurations should be used very carefully.

When the accuracy assessment is carried out over the whole working area (Fig. 5), again higher vertical accuracies, in terms of standard deviation, LE90, and LE95, are yielded by increasing the convergence angle. In this way, it is noteworthy that the five mixed stereo pairs presenting more than 294 days between acquisition dates (i.e., those using the image GE11 that are shown in Fig. 5 as unfilled black circles) are showing the worst vertical accuracies over the whole working area. It is because of the changes happened throughout the time, mainly over agricultural areas, as it will be illustrated later. In the same figure, but regarding the urban area of Villaricos, the relationship between convergence angle and vertical accuracy is not so clear. In addition, there is no difference between stereo pairs whose images are acquired with < 39 days of difference (gray triangles in Fig. 5) and those taken with more than 294 days of difference (unfilled gray triangles in Fig. 5). In other words, changes happened throughout the time did not significantly influence the accuracy attained over urban areas. Last but not least, the percentage of outliers detected by using the three-sigma rule is ranging from 1.13% to 2.29% for all cases tested. In addition, any clear relationship neither with the convergence angle nor with the difference between acquisition dates is detected.

B. DSM Completeness

Fig. 6 shows that, overall, RPC0 model yielded slightly better DSM completeness results than CCRS over the whole

This article has been accepted for inclusion in a future issue of this journal. Content is final as presented, with the exception of pagination.

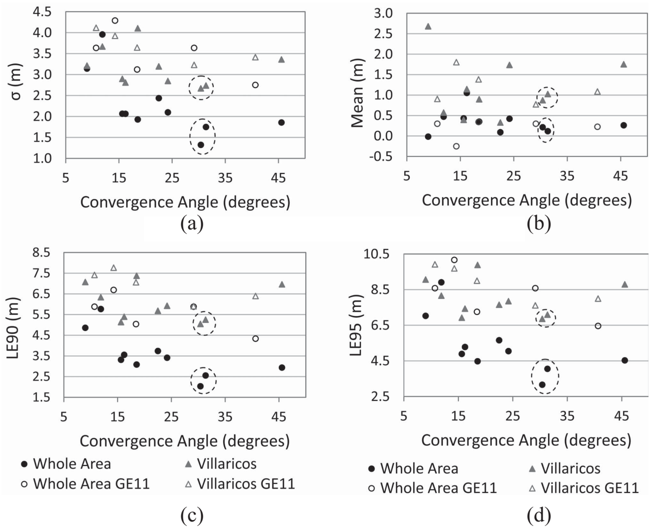

Fig. 5. Relationship between signed z-difference statistics after removing outliers and convergence angle for each stereo pair. (a) Standard deviations. (b) Mean values. (c) 90th percentile linear error. (d) 90th percentile linear error. The presented statistics correspond to the particular urban area of Villaricos or the whole area covered by each stereo pair. z-differences refer to the height difference between each computed DSM from satellite images and the LiDAR elevation data. Pure stereo pairs are highlighted by means of a dashed circle. The five mixed stereo pairs using GE11 image are presented as unfilled figures.

working area. Similar results are reported on IKONOS stereo pairs [15]. However, working on both QuickBird basic stereo products [15] and high resolution Radarsat-2 stereo images [42], CCRS model attained better matching success. It is important that, for the pure stereo pairs, WV2 achieved much better completeness (83.35% for RPC0 model and 81.58% for CCRS) than that provided by GE1 (74.50% for RPC0 model and 73.64% for CCRS). Taking all stereo pairs into consideration, Fig. 6(a) shows that temporal difference between the acquisition dates of the images that form each stereo pair turned out to be the most important factor affecting DSM completeness over the whole working area. The worst results are obtained when the image GE11 (September 2010) is included into the considered stereo pair, which means differences between acquisition dates of 295 days or even more so. Summing up, completeness values are lower when increasing the time difference between the acquisition of the images making up the stereo pair. It is especially clear in very changing areas. However, convergence angle and DSM completeness do not show a clear relationship [Fig. 6(b)]. In this way, Fig. 7 shows DSM completeness (RPC0 model supported by 12 GCPs) by means of the correlation coefficients or score channel computed in the matching process. More white pixels [Fig. 7(b) and (c)] indicate a better correlation coefficient, whereas black pixels are pointing out mismatched points with correlation coefficients < 0.5. It should be noted that, in agricultural areas located at western in Fig. 7, DSM completeness is much better from using same-date images [Fig. 7(b)] than from employing images that differ 324 days regarding acquisition dates [Fig. 7(c)]. The relatively unchanged urban areas located at the northeast of Fig. 7 are not affected by the time difference as severely as agricultural ones.

Fig. 8 shows the relationship between DSM completeness and convergence angle for each land cover. The five stereo

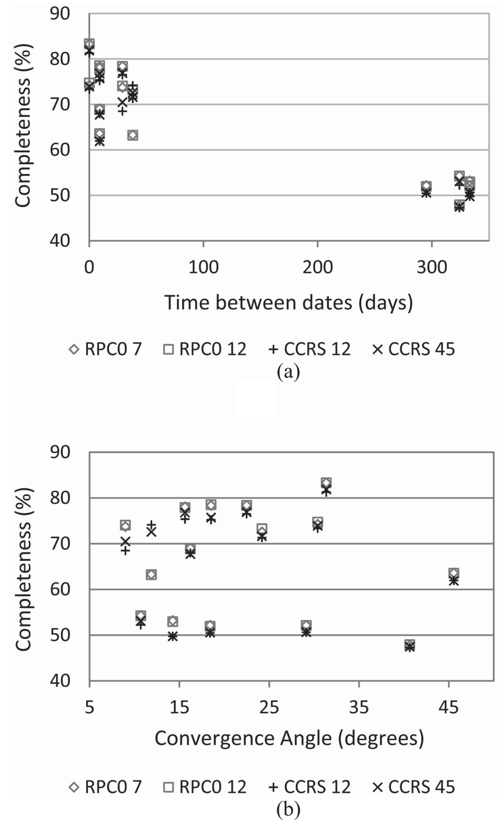

Fig. 6. Completeness for each DSM extracted from VHR satellite stereo pairs over the whole working area depending on (a) the temporal difference between acquisition dates and (b) the convergence angle.

pairs that presented more than 294 days between acquisition dates are previously removed to avoid their strong influence in the results. Likewise RPC0 sensor model supported by 12 GCPs is applied. It can be appreciated that convergence angle did not have any influence on completeness for flat and unchanged areas. In urban areas, DSM completeness is higher when decreasing the convergence angle. Thus, a large convergence angle or B/H ratio cannot be recommended for stereo imaging of urban areas because of the different perspectives resulting in occluded areas and moving shadows from image to image [7], [24]. Regarding the pure stereo pairs, highlighted by means of a dashed ellipse in Fig. 8, again WV2 showed higher completeness than GE1 for both unchanged (77.69% and 73.59%, respectively) and especially urban areas (78.83% and 63.23%).

C. Radiometric Characteristics

In theory, a number of 2048 (11-bit) possible digital numbers (DNs) values could be collected by both GE1 and WV2 sensors. However, a compression of the range of DNs is done on purpose by the imaging companies to account for extremely reflective surfaces that could create flares [48]. DN values rarely exceed 1500 in raw VHR satellite imagery without any especial radiometric correction or contrast enhancement. In GE1 imagery, the 99% of the DNs vary between 110 and 780 [49] whereas the main information is distributed between zero and ten bits for WV2 imagery [50].

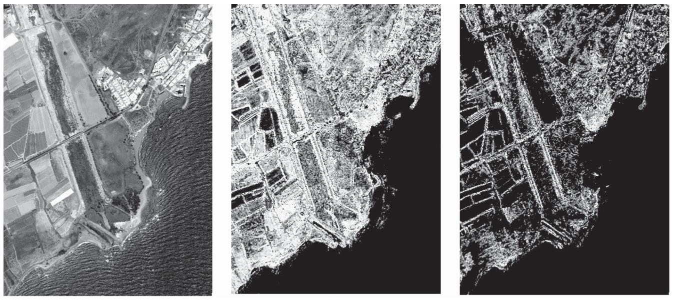

(a) (b) (c)

Fig. 7. Completeness over a limited study area (1160 × 1620 m). (a) WV21 original PAN image. (b) ID 2 DSM score channel. (c) ID 13 DSM score channel.

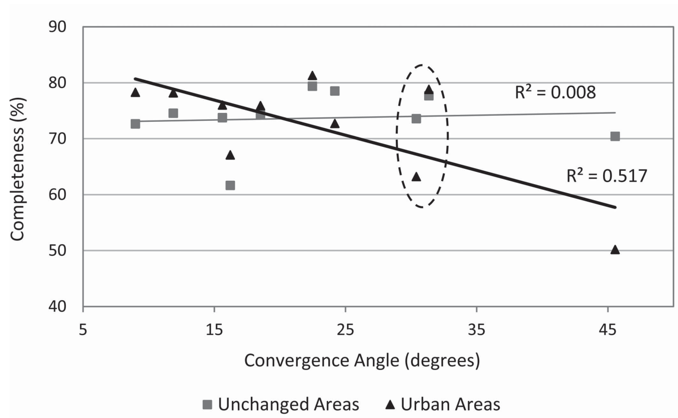

Fig. 8. Completeness for each VHR stereo pair derived DSM over unchanged and urban areas depending on the convergence angle. Linear trend lines. Pure stereo pair results are highlighted by means of a dashed ellipse.

Overall, the peak of the gray level histograms is typically toward the darker values with the right part of the histograms decreasing smoothly and slowly toward the higher DN values [50], [51]. The six DNs histograms corresponding to the tested PAN images (Fig. 9) fit quite well with this typical shape. However, a higher compression of the DNs histograms corresponding to the six original (non-orthorectified) PAN VHR satellite images over the whole working area is observed in the WV2 case (Fig. 9). Fig. 9 shows clear visual differences between the GE12 original PAN image [Fig. 3(a)] and WV23 original one [Fig. 3(b)], the last appearing blurrier and so showing less contrast. This visual effect can also be appreciated in the second figure of the recent paper published by Agugiaro *et al.* [52] over Trento testfield (Italy). The quality of an image may be evaluated by using the amount of blurring at edges. Noise is also an important criterion for measuring image quality. In this sense, to quantify those effects in our datasets, a no-reference image quality assessment using blur ratio ($Blur_{ratio}$) and noise ratio ($Noise_{ratio}$) [53] is carried out over the working area. The $Blur_{ratio}$ indexes computed for the GE1 original PAN images (0.392, 0.389, and 0.496 for GE11, GE12, and GE13, respectively) are much lower than the ones calculated for the WV2 images (0.787, 0.919, and 0.902 for WV21, WV22, and WV23). Those differences are quantitatively confirming what can be visually deduced from Fig. 3(a) and (b). For each sensor, the $Blur_{ratio}$ values are higher with increasing off-nadir angle. In the same way, image blur problem caused by stability incompleteness of the sensor stabilizer is already reported by [54] working on linear array digital images. This problem is more serious on the forward and backward viewing images than on the nadir viewing image. Regarding $Noise_{ratio}$ index, no significant differences are detected between GE1 images (0.375, 0.380, and 0.381) and WV2 ones (0.394, 0.393, and 0.386).

Regarding the pure stereo pairs from GE1 and WV2, note that the vertical accuracy achieved from GE1 DSM is higher than the one attained from WV2, although the DSM completeness for GE1 turned out to be lower than the one provided by WV2 for every studied land cover. The clear visual differences found between the original single images from GE1 and WV2, which can be observed through their DN histograms and by using a quantitative quality index such as $Blur_{ratio}$, could be related to these results. The undergoing hypothesis of this paper is that the observed differences in image quality between each single image from sensors GE1 and WV2 could affect the performance of the digital stereo matching algorithm. In addition, those differences might be because of operational conditions of the image acquisition such as sensor viewing angle, sun acquisition angles, and atmospheric conditions [50]. However, the previously described findings are pointing out to the specific radiometric characteristics of both sensor systems as the most important factor. In that sense, when an automated area-based matching procedure is applied, blurred images could lead to an improvement of the success rate in the matching process, although getting a lower accuracy for the correlated points. Previous works based on the DSM matching principles of OrthoEngine and Leica IMAGINE OrthoBASE (both using a similar area-based matching strategy) revealed that the smoothing effect brings more successful matching pairs but also resulted in more inaccurate matching points in the extracted DSMs [55], [56]. In our case, an evident smoothing effect because of image blurring is detected in WV2 imagery. Fig. 10 shows a clear relationship between completeness over the whole working area and the average value of $Blur_{ratio}$ for the two images making up each stereo pair. The five mixed stereo pairs containing GE11 image are not presented as they could introduce significant errors. It is also worth noting that the imaginary line joining the points corresponding to the pure stereo pairs [GE1 (ID 1) and WV2 (ID 2)] would turn out to be almost parallel to the trend line corresponding to all the presented data (Fig. 10).

Moreover, urban areas presented higher $Blur_{ratio}$ difference between GE1 and WV2 images than non-urban areas. Focusing on Villaricos urban area, the mean $Blur_{ratio}$ for GE1 images is close to 0.326 whereas a value of 0.869 is calculated for WV2 images. Looking at agricultural areas, the mean $Blur_{ratio}$ values took values of 0.725 and 0.989 for GE1 and WV2 images, respectively. Thus, DSM completeness differences in urban areas between GE1 and WV2 pure stereo pairs are also larger than on unchanged zones or over the whole working area. Moreover, it is worth highlighting that the three highest values for DSM completeness in urban areas are computed on DSMs extracted from the three stereo pairs composed of two single WV2 images (i.e., ID 2, 7, and 8).

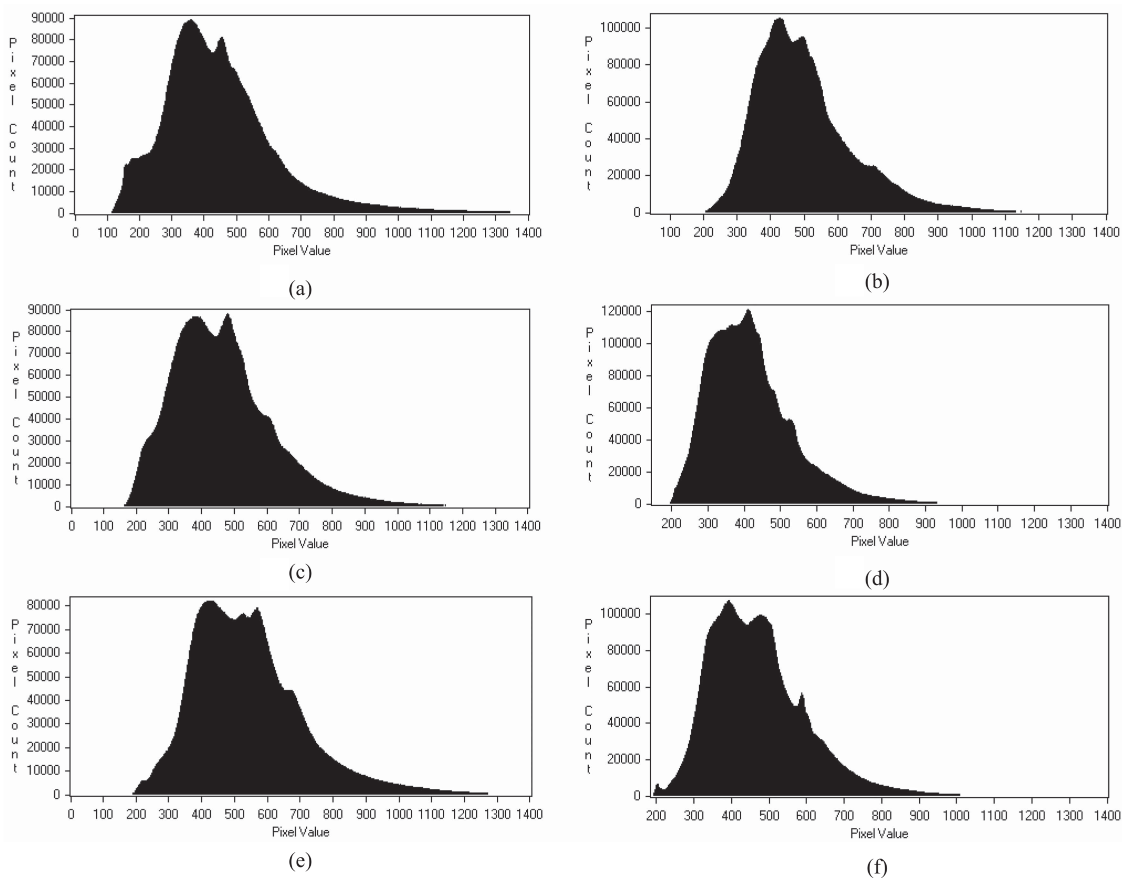

Fig. 9. Histograms of digital numbers from the six PAN VHR satellite images over the whole working area. (a) GE11. (b) WV21. (c) GE12. (d) WV22. (e) GE13. (f) WV23.

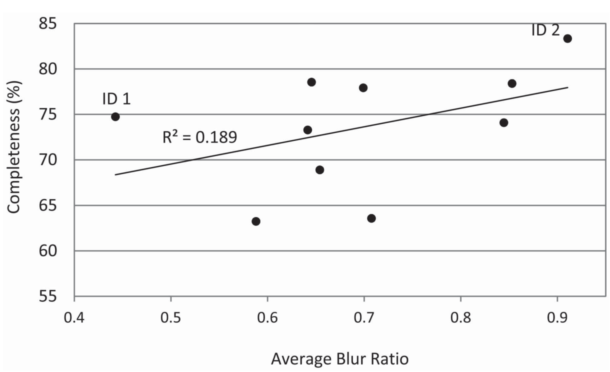

Fig. 10. Relationship between the completeness over the whole area and the average value of Blur ratio for each stereo pair.

All VHR satellites employ TDI technology. This technique for blur-free capture of moving images basically sensed charge patterns and shifted them across the charge-coupled device for attaining the final line. However, the accumulation of the signal with TDI technology leads to a smoothing of the signal, especially in the flight direction, as the TDI lines cannot exactly image the same scene surface and thus a signal mixing occurs [51]. GE1 VHR PAN satellite images used 16 TDI stages whereas WV2 employed 32 TDI stages might be contributing to the observed WV2 blurring effect. In this way, it would be interesting to study whether the differences about image quality between GE1 and WV2 PAN imagery are because of operational conditions regarding image acquisition or they are caused by specific characteristics of both sensor systems. Also, it is extremely important to take this research line on to investigate whether the aforementioned radiometric differences between the tested satellite sensors could actually affect the final DSM vertical accuracy and completeness results when using other image-processing software modules and so applying other image matching algorithms.

V. Conclusion

The DSM vertical accuracy assessment tests carried out over flat and unchanged areas by using different number of GCP and two sensor models, RPC0, and CCRS, resulted in similar standard deviations ranging from 0.39 to 2.07 m. The vertical accuracy computed on this land cover was always higher with increasing convergence angle or B/H ratio. Moreover, vertical systematic errors were too large when a weak stereo pair configuration was used, i.e., with convergence angles $<18°$ (or B/H ratios <0.28). Overall, the quality of the extracted DSMs largely depended on the target land cover, being better for DSMs covering flat areas than those attained over urban areas or the entire working area. Over the whole working area, vertical accuracies ranging from 1.33 (σ), 2.04 (LE90), and 3.16 m (LE95) to 4.29 (σ), 6.69 (LE90), and 10.17 m (LE95) were yielded mainly depending on the stereo pair imaging geometry. However, vertical accuracy over urban areas was not so influenced by the convergence angle, presenting LE90 values within the range of 5.05 and 7.77 m.

Regarding DSM completeness, RPC0 supported by 7 or 12 GCPs was the sensor model that yielded slightly more accurate DSMs, providing DSM completeness values ranging from 47.94% to 83.35%. In this case, temporal difference between the acquisition dates was the most influential factor. As stated previously, these results could be improved through prefiltering the original images comprising each stereo pair. Agricultural areas were the zones most concerned by the last issue. As in DSM completeness in urban areas, convergence angles $< 25°$ should be used to attain more similarity between the two images making up the stereo pairs and, moreover, to avoid occluded areas. The possible effect on DSM vertical accuracy and completeness because of differences in sun positions could not be found, most likely because of it was somehow masked by other stronger factors.

Although DSMs extracted from mixed stereo pairs achieved good quality, the best accuracy was attained for the case of pure along-track same-date stereo pairs. They presented convergence angles close to 30° and the lowest radiometric image variations such as temporal changes and sun illumination. From the last, higher DSMs completeness values were achieved from WV2 (83.35%) as compared with GE1 (74.50%). Simultaneously, and working over unchanged areas, better DSM vertical accuracy (measured as standard deviation) was achieved in GE1 pure stereo pair (0.39 and 0.53 m for GE1 and WV2, respectively). It was likely because of its better contrast and image quality. Focusing in urban areas, notable lower DSM vertical accuracy values (standard deviation) were computed both from GE1 (2.67 m) and WV2 (2.74 m) pure stereo pairs. Finally, DSM vertical accuracy computed over the whole working area produced intermediate but also consistent results, confirming the better overall performance of GE1 stereo pair (1.32 m for GE1 and 1.75 m for WV2). The radiometric differences between WV2 and GE1 PAN single images highlighted in this paper, being WV2 images clearly blurrier than GE1 ones, was proposed as the main cause for these findings.

ACKNOWLEDGMENT

The authors would like to thank M. Palenzuela for contributions to this paper, as well as the kind and valuable comments and suggestions made by three anonymous reviewers are also much appreciated.

REFERENCES

[1] S. Kay, P. Spruyt, and K. Alexandrou, "Geometric quality assessment of orthorectified VHR space image data," *Photogramm. Eng. Remote Sens.*, vol. 69, no. 5, pp. 484–491, 2003.

[2] C. H. Davis and X. Wang, "Planimetric accuracy of Ikonos 1 m panchromatic orthoimage products and their utility for local government GIS basemap applications," *Int. J. Remote Sens.*, vol. 24, no. 22, pp. 4267–4288, Nov. 2003.

[3] M. A. Aguilar, F. J. Aguilar, F. Agüera, and J. A. Sánchez, "Geometric accuracy assessment of QuickBird basic imagery using different operational approaches," *Photogramm. Eng. Remote Sens.*, vol. 73, no. 12, pp. 1321–1332, Dec. 2007.

[4] M. A. Aguilar, F. Agüera, F. J. Aguilar, and F. Carvajal, "Geometric accuracy assessment of the orthorectification process from very high resolution satellite imagery for Common Agricultural Policy purposes," *Int. J. Remote Sens.*, vol. 29, no. 24, pp. 7181–7197, Nov. 2008.

[5] T. Toutin, "Comparison of stereo-extracted DTM from different high-resolution sensors: SPOT-5, EROS-a, IKONOS-II, and QuickBird," *IEEE Trans. Geosci. Remote Sens.*, vol. 42, no. 10, pp. 2121–2129, Oct. 2004.

[6] J. Poon, C. S. Fraser, and C. Zhang, "Digital surface models from high resolution satellite imagery," *Photogramm. Eng. Remote Sens.*, vol. 73, no. 11, pp. 1225–1232, Nov. 2007.

[7] S. Eckert and T. Hollands, "Comparison of automatic DSM generation modules by processing IKONOS stereo data of an urban area," *IEEE J. Sel. Topics Appl. Earth Observat. Remote Sens.*, vol. 3, no. 2, pp. 162–167, Jun. 2010.

[8] K. Deilami and M. Hashim, "Veryhigh resolution optical satellites for DEM generation: A review," *Eur. J. Sci. Res.*, vol. 49, no. 4, pp. 542–554, 2011.

[9] P. Capaldo, M. Crespi, F. Fratarcangeli, A. Nascetti, and F. Pieralice, "DSM generation from high resolution imagery: Applications with WorldView-1 and GeoEye-1," *Ital. J. Remote Sens.*, vol. 44, no. 1, pp. 41–53, Jan. 2012.

[10] R. Li, F. Zhou, X. Niu, and K. Di, "Integration of Ikonos and QuickBird imagery for geopositioning accuracy analysis," *Photogramm. Eng. Remote Sens.*, vol. 73, no. 9, pp. 1067–1074, 2007.

[11] R. Li, X. Niu, C. Liu, B. Wu, and S. Deshpande, "Impact of imaging geometry on 3D geopositioning accuracy of stereo Ikonos imagery," *Photogramm. Eng. Remote Sens.*, vol. 75, no. 9, pp. 1119–1125, 2009.

[12] T. Toutin, "Elevation modeling from satellite data," in *Encyclopedia Analytical Chemistry: Applications, Theory and Instrumentation*, R. A. Meyers, Ed. New York, USA: Wiley, 2000, pp. 8543–8572.

[13] C. S. Fraser, E. Baltsavias, and A. Gruen, "Processing of Ikonos imagery for submetre 3D positioning and building extraction," *ISPRS J. Photogramm. Remote Sens.*, vol. 56, no. 3, pp. 177–194, Mar. 2002.

[14] T. Toutin, "Error tracking in Ikonos geometric processing using a 3D parametric model," *Photogramm. Eng. Remote Sens.*, vol. 69, no. 1, pp. 43–51, Jan. 2003.

[15] T. Toutin, "Comparison of 3D physical and empirical models for generating DSMs from stereo HR Images," *Photogramm. Eng. Remote Sens.*, vol. 72, no. 5, pp. 597–604, 2006.

[16] C. S. Fraser and M. Ravanbakhsh, "Georeferencing accuracy of GeoEye-1 imagery," *Photogramm. Eng. Remote Sens.*, vol. 75, no. 6, pp. 634–638, 2009.

[17] D. Poli, "Modelling of spaceborne linear array sensors," Ph.D. dissertation, nstitut für Geodäsie und Photogrammetrie an der Eidgenössischen, Technische Wissenschaften ETH Zurich, Zurich, Switzerland, 2005.

[18] M. Crespi, F. Fratarcangeli, F. Giannone, and F. Pieralice, *High Resolution Satellite Image Orientation Models: Geospatial Technology for Earth Observation*, D. Li, J. Shan, and J. Gong, Eds. New York, USA: Springer-Verlag, 2009, pp. 63–104.

[19] M. Crespi, F. Fratarcangeli, F. Giannone, and F. Pieralice, "A new rigorous model for high-resolution satellite imagery orientation: Application to EROS A and QuickBird," *Int. J. Remote Sens.*, vol. 33, no. 8, pp. 2321–2354, 2012.

[20] X. Yuan, *Geometric Processing Models for Remotely Sensed Imagery and their Accuracy Assessment: Geospatial Technology for Earth Observation*, D. Li, J. Shan, and J. Gong, Eds. New York, USA: Springer-Verlag, 2009, pp. 105–139.

[21] K. Jacobsen, M. Crespi, F. Fratarcangeli, and F. Giannone, "DEM generation with CARTOSAT-1 Stereo Imagery," in *Proc. EARSeL Joint Workshop Remote Sens., New Challenges High Resolut.*, Mar. 2008, pp. 5–7.

[22] P. J. Åstrand, M. Bongiorni, M. Crespi, F. Fratarcangeli, J. N. Da Costa, F. Pieralice, and A. Walczynska, "The potential of WorldView-2 for ortho-image production within the 'Control with Remote Sensing Programme' of the European Commission," *Int. J. Appl. Earth Obs., Geoinf.*, vol. 19, pp. 335–347, Oct. 2012.

[23] L. Zhang and A. Gruen, "Multi-image matching for DSM generation from IKONOS imagery," *ISPRS J. Photogramm. Remote Sens.*, vol. 60, no. 3, pp. 195–211, May 2006.

[24] A. Alobeid, K. Jacobsen, and C. Heipke, “Comparison of matching algorithms for DSM generation in urban areas from IKONOS imagery,” *Photogramm. Eng. Remote Sens.*, vol. 76, no. 9, pp. 1041–1050, 2010.

[25] G. Mitchell and K. MacNabb, “High resolution stereo satellite elevation mapping accuracy assessment,” in *Proc. Annu. ASPRS Conf.*, Apr. 2010, pp. 1–12.

[26] W. Wang and L. Zhao, “Geolocation accuracy evaluation of GeoEye-1 stereo image pair,” in *Proc. Int. Symp. Image Data Fusion*, Aug. 2011, pp. 1–4.

[27] Y. Meguro and C. S. Fraser, “Georeferencing accuracy of GeoEye-1 stereo imagery: Experiences in a Japanese test field,” in *Proc. Int. Archives Photogramm., Remote Sens. Spatial Inf. Sci.*, vol. 38, no. 8, pp. 1069–1072, Aug. 2010,

[28] M. L. Hobi and C. Ginzler, “Accuracy assessment of digital surface models based on WorldView-2 and ADS80 stereo remote sensing data,” *Sensors*, vol. 12, no. 5, pp. 6347–6368, May 2012.

[29] F. J. Aguilar and J. P. Mills, “Accuracy assessment of Lidar-derived digital elevation models,” *Photogramm. Rec.*, vol. 23, no. 122, pp. 148–169, 2008.

[30] J. Höhle and M. Höhle, “Accuracy assessment of digital elevation models by means of robust statistical methods,” *ISPRS J. Photogramm. Remote Sens.*, vol. 64, no. 4, pp. 398–406, Jul. 2009.

[31] F. J. Aguilar, F. Agüera, M. A. Aguilar, and F. Carvajal, “Effects of terrain morphology, sampling density, and interpolation methods on Grid DEM accuracy,” *Photogramm. Eng. Remote Sens.*, vol. 71, no. 7, pp. 805–816, Jul. 2005.

[32] Z. Li, “Variation of the accuracy of digital terrain models with sampling interval,” *Photogramm. Rec.*, vol. 14, no. 79, pp. 113–128, Jul. 1992.

[33] J. Poon, C. S. Fraser, Z. Chunsun, Z. Li, and A. Gruen, “Quality assessment of digital surface models generated from IKONOS imagery,” *Photogramm. Rec.*, vol. 20, no. 110, pp. 162–171, Jun. 2005.

[34] J. B. Butler, S. N. Lane, and J. H. Chandler, “Assessment of DEM quality for characterizing surface roughness using close range digital photogrammetry,” *Photogramm. Rec.*, vol. 16, no. 92, pp. 271–291, Jan. 1998.

[35] J. Höhle and M. Potuckova, “The EuroSDR test: Checking and improving of digital terrain models,” in *Proc. Eur. Spatial Data Res.*, 2006, pp. 9–141.

[36] F. J. Aguilar, F. Agüera, and M. A. Aguilar, “A theoretical approach to modeling the accuracy assessment of Digital Elevation Models,” *Photogramm. Eng. Remote Sens.*, vol. 73, no. 12, pp. 1367–1379, Jan. 2007.

[37] GeoEye, Inc. (2009). *GeoEye Product Guide*, Herndon, VA, USA [Online]. Available: http://www.geoeye.com/CorpSite/assets/docs/brochures/GeoEye_Product_Guide.pdf

[38] DigitalGlobe, Inc. (2010). *DigitalGlobe Core Imagery Products Guide*, Longmont, CO, USA [Online]. Available: http://www.digitalglobe.com/downloads/DigitalGlobe_Core_Imagery_Products_Guide.pdf

[39] P. Chen and C. Chaapel, “Automatic DEM generation using WorldView-1 stereo data with or without ground control,” *GeoInformatics*, vol. 7, pp. 34–39, May 2008.

[40] M. A. Aguilar, M. M. Saldaña, and F. J. Aguilar, “Assessing geometric accuracy of the orthorectification process from GeoEye-1 and WorldView-2 panchromatic images,” *Int. J. Appl. Earth Obs. Geoinf.*, vol. 21, pp. 427–435, Apr. 2013.

[41] J. Grodecki and G. Dial, “Block adjustment of high-resolution satellite images described by rational polynomials,” *Photogramm. Eng. Remote Sens.*, vol. 69, no. 1, pp. 59–68, Jan. 2003.

[42] T. Toutin, “Radarsat-2 DSM generation with new hybrid, deterministic, and empirical geometric modeling without GCP,” *IEEE Trans. Geosci. Remote Sens.*, vol. 50, no. 5, pp. 2049–2055, May 2012.

[43] C. Daniel and K. Tennant, *DEM quality Assessment, Digital Elevation Model Technologies and Applications: The DEM Users Manual*, D. F. Maune, Ed. Bethesda, MD, USA: ASPRS, 2001, pp. 395–440.

[44] M. A. Aguilar, F. J. Aguilar, M. M. Saldaña, and I. Fernández, “Geopositioning accuracy assessment of GeoEye-1 panchromatic and multispectral imagery,” *Photogramm. Eng. Remote Sens.*, vol. 78, no. 3, pp. 247–257, 2012.

[45] H. Hirschmüller, “Stereo processing by semiglobal matching and mutual information,” *IEEE Trans. Pattern Anal. Mach. Intell.*, vol. 30, no. 2, pp. 328–341, Feb. 2008.

[46] S. Birchfield and C. Tomasi, “A pixel dissimilarity measure that is insensitive to image sampling,” *IEEE Trans. Pattern Anal. Mach. Intell.*, vol. 20, no. 4, pp. 401–406, Apr. 1998.

[47] M. Crespi, L. De Vendictis, D. Poli, K. Wolff, G. Colosimo, A. Gruen, and F. Volpe, “Radiometric quality and DSM generation analysis of Cartosat-1 stereo imagery,” *Int. Arch. Photogramm. Remote Sens. Spatial Inf. Sci.*, vol. 37 no. 3, pp. 1349–1355, Mar. 2008.

[48] B. A. McCarty. (2010). *Word of the Month—Bit Depth*. eMap International’s GeoViews, Reddick, FL, USA [Online]. Available: http://www.emap-int.com/2010/June/article8.html

[49] M. Crespi, G. Colosimo, L. De Vendictis, F. Fratarcangeli, and F. Pieralice, “GeoEye-1: Analysis of radiometric and geometric capability,” in *Proc. 2nd Int. ICST Conf., Pers. Satellite Services*, Feb. 2010, pp. 354–369.

[50] D. Poli, E. Angiuli, and F. Remondino, “Radiomeric and geometric analysis of WorldView-2 stereo scenes,” *Int. Archives Photogramm., Remote Sens. Spatial Inf. Sci.*, vol. 38, no. 1, pp. 1–6, Jun. 2010.

[51] E. Baltsavias, M. Pateraki, and L. Zhang, “Radiometric and geometric evaluation of IKONOS Geo images and their use for 3D building modeling,” in *Proc. ISPRS Workshop High Resolut. Mapping Space*, Sep. 2001, pp. 1–21.

[52] G. Agugiaro, D. Poli, and F. Remondino, “Testfield Trento: Geometric evaluation of very high resolution satellite imagery,” *Int. Archives Photogramm., Remote Sens. Spatial Inf. Sci.*, vol. 39, no. 8, pp. 1–6, Aug.–Sep. 2012.

[53] M. G. Choi, J. H. Jung, and J. W. Jeon, “No-reference image quality assessment using blur and noise,” *Int. J. Electr. Electron. Eng.*, vol. 3, no. 6, pp. 318–322, 2009.

[54] L. Zhang, “Automatic digital surface model (DSM) generation from linear array images,” Ph.D. dissertation, Inst. Geodesy Photogramm., Swiss Federal Institute of Technology ETH Zurich, Zurich, Switzerland, 2005.

[55] J. K. Liu, J. H. Wu, and T. Y. Shih, “Effects of JPEG2000 on the information and geometry content of aerial photo compression,” *Photogramm. Eng. Remote Sens.*, vol. 71, no. 2, pp. 157–167, Feb. 2005.

[56] T. Y. Shih and J. K. Liu, “Effects of JPEG 2000 compression on automated DSM extraction: Evidence from aerial photographs,” *Photogramm. Rec.*, vol. 20, no. 112, pp. 351–365, Dec. 2005.

Manuel Ángel Aguilar received the Agricultural Engineering degree and the Dr.Ing. degrees from the University of Córdoba, Córdoba, Spain, in 1996 and 2001, respectively.

He has been a Professor of drawing engineering with the Almería Engineering High School, University of Almería, Almería, Spain, since 1999, after two years with a Spanish engineering company. He is currently a Senior Lecturer with the University of Almería, working with the Department of Engineering. Recently, he has led same research projects based on very high resolution commercial satellite imagery (mainly IKONOS, QuickBird, GeoEye-1 and WorldView-2) where the aims were sensor orientations for single and stereo images, ortorectification stage, classification of land cover, as well as the generation and quality control of DSMs. His current research project is focused on the latest breed of Very High Resolution satellite imagery. His current research interests include close-range, airborne, and spaceborne VIR digital photogrammetry.

María del Mar Saldaña received the Technical Engineers in Topography degree from the University of Jaén, Jaén, Spain, in 2009, and the Master's degree from the University of Almeria, Almeria, Spain, in 2011, attaining the Award for the best work presented within the Master's in engineering applied máster from Almería University. She is currently pursuing the Ph.D. degree with the Department of Agricultural Engineering, University of Almería, under a research project with the support of the Spanish Ministry for Science and Innovation (Spanish Government) and the European Union (FEDER founds) under Grant Reference CTM2010-16573.

Her current research interest include topography, remote sensing, satellite and classic digital photogrammetry, generation and quality control DEMs and orthophotos with the most innovative very high resolution satellite imagery such as GeoEye-1 and WorldView-2.

Fernando José Aguilar received the Ph.D. degree from Cordoba University, Cordoba, Spain, in 1997.

He is currently a Senior Lecturer with the Department of Agricultural Engineering Almeria University, Almeria, Spain. He is currently the Head of the Researh Group "Integrated Landscape Management and Spatial Informacion Technologies," leading an Excellence Research Project entitled *Multisource geospatial data integration and mining for the monitoring and modelling of coastal areas evolution and vulnerability*. He has authored several international publications and also a peer-reviewer of main GIS and Remote Sensing journals all over the world. His current research interests include digital elevation models, remote sensing, digital photogrammetry, and GIS.